Impact of the seasonal variations of composition on the temperature field of Titan's stratosphere

Sébastien Lebonnois,[a,*] Frédéric Hourdin,[a] Pascal Rannou,[b] David Luz,[c] and Dominique Toublanc[d]

[a] *Laboratoire de Météorologie Dynamique, IPSL, CNRS/UPMC, Box 99, F-75252 Paris Cedex 05, France*
[b] *Service d' Aéronomie, IPSL, CNRS/UVSQ, Verrières-le-Buisson, France*
[c] *Centro de Astronomia e Astrofísica da Universidade de Lisboa, Observatório Astronómico de Lisboa, Lisboa, Portugal*
[d] *Centre d'Etude Spatiale des Rayonnements, CNRS/UPS, Toulouse, France*

Received 22 March 2002; revised 30 January 2003

Abstract

We investigate the role of seasonal variations of Titan's stratospheric composition on the temperature. We use a general circulation model coupled with idealized chemical tracers that reproduce variations of ethane (C_2H_6), acetylene (C_2H_2), and hydrogen cyanide (HCN). Enhancement of the mole fractions of these compounds, at high latitudes in the winter hemisphere relative to their equatorial values, induces a relative decrease in temperature above approximately 0.2 mbar, with a peak amplitude around −20 K, and a relative increase in temperature below, around 1 mbar, with a peak amplitude around +7 K. These thermal effects are mainly due to the variations of the cooling to space induced by the varying distributions. The ethane, acetylene, and hydrogen cyanide variations affect the cooling rates in a similar way, with the dominant effect being due to ethane, though its latitudinal variations are small.

Keywords: Titan; Atmospheres, composition; Radiative transfer

1. Introduction

Titan's stratospheric composition has been deduced from IRIS/Voyager 1 spectra by Coustenis and co-workers (Coustenis et al., 1989, 1991; Coustenis and Bézard, 1995), for different latitudes, in the 100- to 150-km altitude range (located in the lower stratosphere). At the time of Voyager 1 fly-by (November 1980), Titan was close to northern spring equinox (solar longitude $L_S = 9°$). Latitudinal variations were observed in the composition, with an enrichment of most observed species at high northern latitudes (Coustenis and Bézard, 1995). These variations were recently interpreted as an effect of transport by the meridional circulation (Lebonnois et al., 2001), using a 2-dimensional photochemical model with a stratospheric circulation obtained from a general circulation model (GCM) of Titan's atmosphere (Hourdin et al., 1995). The polar enrichment was shown to be caused by subsiding air coming from the mesosphere where photochemistry is most active.

Using IRIS/Voyager 1 spectra, latitudinal profiles of the temperature were also obtained for different pressure levels (Flasar and Conrath, 1990; Coustenis and Bézard, 1995). In the troposphere, the temperature appears to be only slightly dependent on latitude, but in the stratosphere, temperature decreases from equator to pole, and a north-to-south asymmetry is visible. Considering the symmetric insolation pattern at the time of the Voyager 1 fly-by, Flasar and Conrath (1990) suggested that the observed asymmetry was due to dynamical inertia. Using a simple zonally symmetric model, they proposed that the redistribution of axial angular momentum induces a phase lag in the response of the atmosphere to the insolation and therefore could account for the temperature asymmetry. Since this model assumes that the distribution of opacity sources is symmetric with latitude, Bézard et al. (1995) discussed the possibility that this asym-

* Corresponding author. Fax: +33-1-44-27-62-72.
E-mail address: sllmd@lmd.jussieu.fr (S. Lebonnois).

metry is due to latitudinal variations in the atmospheric composition and haze, rather than to a purely dynamical effect. These latitudinal variations, which were observed by Voyager 1, modify both the cooling and the heating rates in the stratosphere. Bézard et al. (1995) calculated these rates at two symmetrical latitudes (50°N and 53°S) using two selections of IRIS spectra and considering different haze models. They concluded that the latitudinal variations in the composition and in the haze distribution between those two locations could account for the observed north-to-south temperature asymmetry. They note though that this complex problem should be investigated with a general circulation model.

Using such a model for Titan's atmosphere, Hourdin et al. (1995) showed that a purely radiative-convective simulation could produce a significant equator-to-pole contrast at equinox and also a significant north-to-south asymmetry, despite the short radiative time constants in the stratosphere. With a complete 3-dimensional dynamical simulation, however, both the equator-to-pole contrast and the north-to-south asymmetry were greatly reduced. In this model, the opacity sources were kept uniform in latitude. Hourdin et al. (1995) suggested that latitudinal variations of both the atmospheric composition and the haze distribution may explain the discrepancy between the dynamical simulation and the observations. The seasonal variations of the aerosols' distribution were recently studied with a coupled general circulation and microphysical model by Rannou et al. (2002a,b). The general circulation model has been modified to a 2-dimensional axi-symmetric version. Non-axi-symmetric planetary waves that do influence the global circulation have been parameterized and the 2-dimensional model produces very similar simulations compared to the full 3-dimensional version. The coupling between dynamics and aerosols is very strong, and it can help interpret many features in the haze layer. The latitudinal temperature profile in the stratosphere is fairly reproduced with this model. Both the vertical structure of the main haze layer and the latitudinal variations in the haze distribution have a major impact on the thermal structure of the stratosphere, and the resulting meridional distribution is responsible for the significant equator-to-pole contrast.

The purpose of the present study is to complete this work by investigating the impact of the variations of composition on the temperature field. In our study of the impact of dynamics on composition (Lebonnois et al., 2001), we demonstrated that the transport of chemical species by the meridional winds was able to reproduce the observed latitudinal variations of composition, in particular the enrichment in north polar latitudes. We investigate now the radiative retroaction of the variations in the meridional composition on the temperature. In the Titan GCM developed at the Laboratoire de Météorologie Dynamique (Hourdin et al., 1995; Luz et al., 2002; Rannou et al., 2002a,b), ethane (C_2H_6), and acetylene (C_2H_2), as well as the major compounds of the atmosphere that are homogeneously distributed in the stratosphere (N_2, CH_4, and H_2), are taken into account in the calculation of the cooling rates (Hourdin et al., 1995; McKay et al., 1989).

To reproduce the variations of the distributions of ethane and acetylene without introducing the whole photochemical model, we used the technique of idealized tracers, as described in Lebonnois et al. (2001). In this technique, the complex photochemistry is replaced for each tracer by a simple linear relaxation toward a prescribed vertical profile. The reasons for this choice are both practical and physical. First, the idealized tracers have been shown to give results very close to the simulations with full chemistry, for the species needed for the purpose of this study. This is due to the fact that below the main production region, the meridional distribution is mainly determined by vertical advection of richer air from above or clear air from below. The second reason for choosing the idealized tracers is the large computational cost of running interactively the chemistry on a 2-dimensional grid with 40 chemical compounds and 284 reactions. Finally, the idealized tracers allow the absolute concentrations to be tuned with respect to Voyager observations, and the amplitude of the latitudinal contrast, by adjusting the vertical relaxation profile. This tuning allows us to predict a thermal forcing by chemistry associated with stratospheric concentrations that are consistent with the analysis of Voyager observations. The model is described in Section 2, together with the simulations of Titan's stratosphere that we conducted. The results concerning the temperature field are described and discussed in Section 3. In Section 4, we discuss the possible effect of including HCN in the radiative calculations.

2. Description of the model

2.1. Idealized tracers in the general circulation model

The version of the GCM we use is based on a 2-dimensional version of a 3-dimensional Titan GCM (Hourdin et al., 1995). Rannou et al. (2002a,b) have included the coupling between dynamics and the microphysical model developed by Cabane, Rannou, and co-workers (Cabane et al., 1993; Rannou et al., 1995). This coupling is strong, and it can successfully explain the main features of the haze layer as results of the interactions between the haze particles and the winds. To improve the 2-dimensional axi-symmetric version of this model, Luz et al. (2002) have modified the parameterization of the horizontal dissipation, including a parameterization of barotropic waves. The model we use in the work described here is based on this latest version of the GCM.

The model extends from the surface up to approximately 1 μbar. It does not include any non-LTE calculations. As shown by Roger Yelle (1991), this approximation should affect the thermal structure above a few μbar. Due to this

limitation, caution should be taken in analyzing GCM results in the uppermost levels (above $\sim$10 μbar).

The calculation of the radiative forcing in the GCM was first described by Hourdin et al. (1995) and is based on the spectrally resolved radiative model by McKay et al. (1989). In the visible (24 spectral intervals), the model accounts for scattering and absorption by haze, Rayleigh scattering, and absorption by CH_4. In the thermal infrared (46 spectral intervals), the opacity sources in the gas phase are dominated by the collision-induced absorption of pairs of N_2, CH_4, and H_2 (McKay et al., 1989), which are the major compounds of the gas phase and are homogeneously distributed in the stratosphere. Gas phase molecules, essentially C_2H_6 (740–940 cm^{-1}) and C_2H_2 (645–815 cm^{-1}), are also significant opacity sources. The treatment of the haze opacity has been updated in the GCM (Rannou et al., 2002a,b). Ethane and acetylene vertical profiles have been taken as uniform in latitude in previous simulations (Hourdin et al., 1995; Rannou et al., 2002a,b; Luz et al., 2002), and the effects of other trace species have been neglected.

In the present study, we reproduce the observed latitudinal variations of the mole fractions of ethane and acetylene (Coustenis and Bézard, 1995) within the GCM, and we study their effects on the temperature field. Due to their high enrichment in high-latitude winter conditions, other compounds are suspected to have a seasonal impact on the radiative transfer, especially HCN (hydrogen cyanide) and C_4H_2 (diacetylene). Including these species in the radiative calculations in the GCM is not straightforward, due to the approach used. The case of HCN will be discussed in Section 4.

Though Lebonnois et al. (2001) used an analytical description of the circulation (derived from Hourdin et al., 1995), the structure of this circulation for all GCM simulations developed by our group is qualitatively similar to this analytical description. The main difference is a reinforcement of the meridional circulation due to the coupling between aerosols and dynamics. The treatment of horizontal dissipation has also been improved, but the role of dynamics on compounds' distributions in the model described here is very similar to the description done in Lebonnois et al. (2001). The meridional circulation is mostly a pole-to-pole Hadley cell with ascending (respectively subsiding) motions in the summer (respectively winter) hemisphere, with a rapid transition around the equinoxes giving rise to a two-cell pattern. Due to this circulation, the air located in the high stratosphere (richer in most compounds than in the low stratosphere) induces an enrichment of the lower stratosphere in the subsiding region. Therefore vertical contrasts imposed by chemistry induce latitudinal contrasts with enrichment toward the winter pole.

2.2. Simulations

The initial state of the atmosphere (baseline) was taken from the simulations conducted by Luz et al. (2002). In these simulations, ethane and acetylene were fixed in the radiative calculations, as in Hourdin et al. (1995). The coupling with the haze was on. We kept this coupling with the haze on, but we also coupled composition and dynamics by taking into account the varying distributions of ethane and acetylene in the radiative calculations.

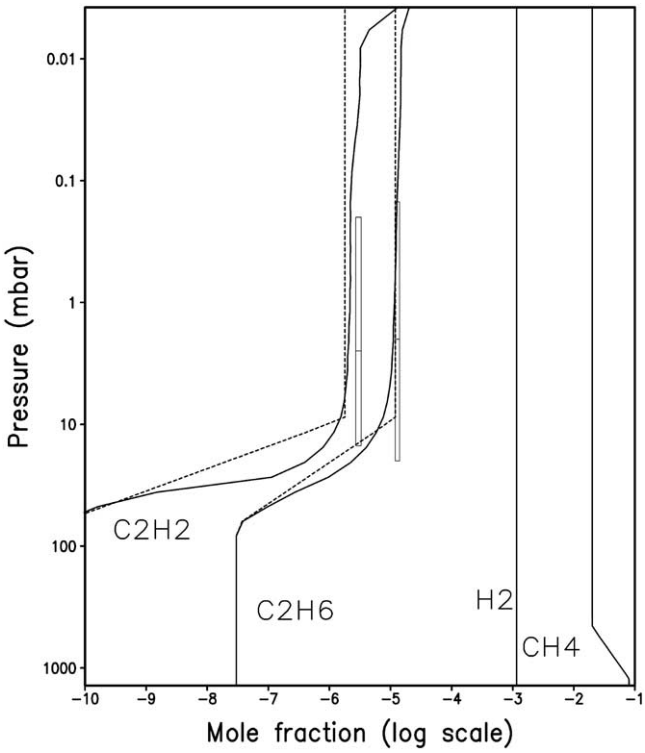

Fig. 1. Vertical profiles of methane, molecular hydrogen, ethane, and acetylene for simulation C (at equator and northern spring equinox, solid line), and simulation R (ethane and acetylene, uniform in latitude, dotted line). A log scale is used for mole fractions: $y = 10^x$.

From the baseline state, we conducted two simulations that were run for the same length of time. The first simulation (simulation R., for *reference*) is done with the ethane and acetylene mole fractions equal to the values used in our previous GCM studies: $y_{C_2H_6} = 1.2 \times 10^{-5}$ and $y_{C_2H_2} = 1.8 \times 10^{-6}$ above their respective condensation levels (these values were primarily used in McKay et al.'s (1989) thermal model). This reference simulation is identical to the simulations of Luz et al. (2002). In the second simulation, C_2H_6 and C_2H_2 are coupled to the dynamics. We let the simulation run until the distributions reached a steady seasonal cycle (seven Titan years). The resulting atmosphere is labeled simulation C, for *coupled.* The vertical profiles of chemical compounds of this coupled simulation (at spring equinox) are close to the values used in simulation R (Fig. 1).

The impact of dynamics on the distributions of ethane and acetylene is illustrated in Fig. 2, at northern spring equinox (simulation C). These distributions reverse just after the equinox and remain fairly stable from mid-spring until the next equinox.

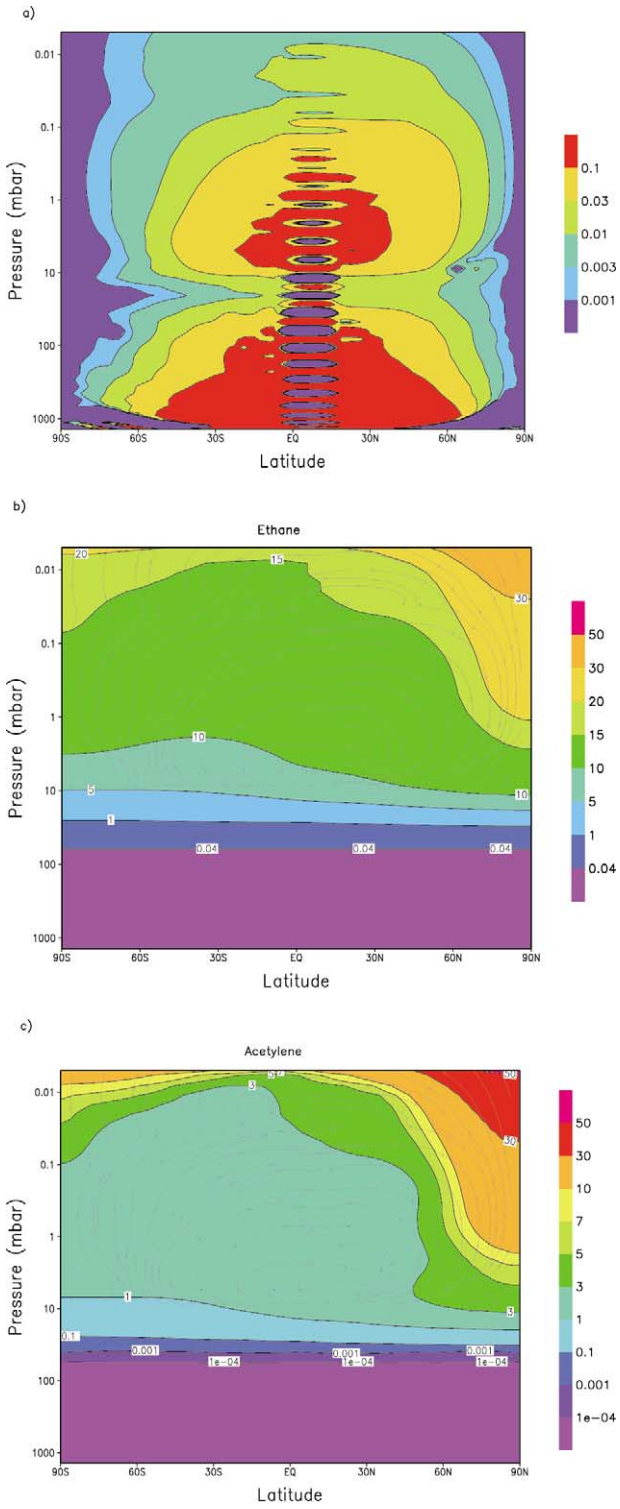

Fig. 2. (a) Meridional stream function, averaged over the period (northern winter solstice, northern spring equinox). Positive values indicate a clockwise circulation, with ascending (respectively subsiding) motion in the southern (respectively northern) hemisphere (unit is 10^9 kg s^{-1}). The oscillations seen between 0 and 15°N in the winter hemisphere have a physical basis. They are related to inertial instability in the tropics, caused by the strong winter jet (Luz et al., 2002). (b, c) Ethane and acetylene meridional distributions (in ppm) at northern spring equinox, for simulation C. The arrows displayed are illustrative of the stream function.

The comparison with the latitudinal profiles retrieved from IRIS/Voyager 1 spectra is shown in Fig. 3. The latitudinal profiles of the mole fractions compare qualitatively well to IRIS data, which is an indirect argument in favor of the stratospheric dynamics modeled in the GCM being close to the actual dynamics in Titan's atmosphere. As indicated previously, the vertical gradient of the relaxation profiles were adjusted to improve the magnitude of the latitudinal contrasts with respect to Voyager. This approach was privileged here since our goal is not to assess our representation of chemistry but rather to evaluate the feedback of latitudinal contrasts on the atmospheric structure. This does not affect the general results of this study, but allows us to obtain temperature effects that should be close to the actual situation in the stratosphere of Titan. The latitudinal contrasts we obtain directly within the GCM are also similar to those obtained with the 2-dimensional photochemical model (Lebonnois et al., 2001), both with all the photochemistry and with the *idealized tracers.* Note, however, that the latitudinal contrast at 60°N is more pronounced than in Lebonnois et al. (2001), in better agreement with observations. This is mainly due to the interactive parameterization used for latitudinal mixing in the GCM. In previous studies, the mean meridional circulation from the GCM was used to transport chemical compounds together with a uniform latitudinal mixing aimed to represent transport by large scale planetary waves. In the present model, the mixing is parameterized using a diffusivity which depends on the dynamical stability of the mean flow (Luz et al., 2002). Mixing is more intense where the flow is more unstable, in particular on the equatorward flank of the winter jet. Hence, between northern winter solstice and equinox (Voyager encounter), the air on the south side of the jet is strongly mixed with the relatively clear air from lower latitudes, but remains isolated from the enriched air subsiding in the polar region, leading to more pronounced contrasts at high latitudes.

3. Results

3.1. Effects of the variations of composition on the temperature field

Fig. 4 shows δT_{CR}, the difference between T_C (temperature field for the coupled simulation) and T_R (for the reference) at the northern spring equinox. Also shown are the differences (in percentages) in ethane mole fraction, $\delta y_{C_2H_6,CR} = 100 \times (y_{C_2H_6,C} - y_{C_2H_6,R})/y_{C_2H_6,R}$, and the temperature field T_C. As discussed in Section 3.2, the variations of both ethane and acetylene induce the thermal effects obtained. Several effects are visible in Fig. 4. First, in the low stratosphere (pressure between 100 and 10 mbar, altitude between 50 and 100 km, approximately), the temperature field is significantly sensitive to the composition in this region. But it must be noted that both the vertical gradients in temperature and the vertical gradient in ethane

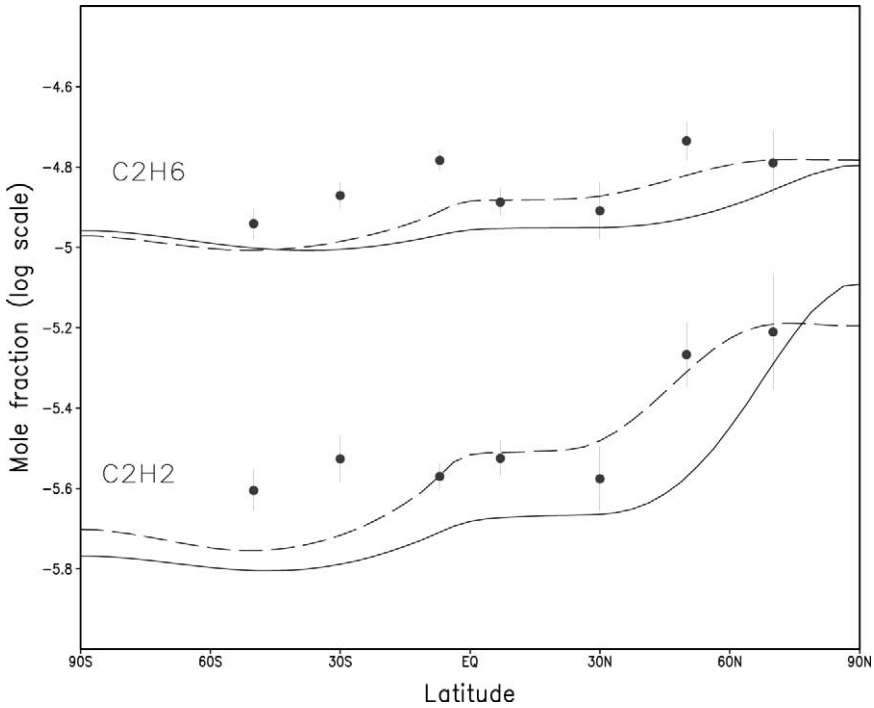

Fig. 3. Latitudinal profiles of ethane and acetylene at a pressure level around 2 mbar (simulation C, solid lines) are compared with the analysis of the IRIS spectra (circles with error bars, Coustenis and Bézard, 1995) for northern spring equinox. Also plotted are the latitudinal profiles for northern winter solstice (dashed lines).

and acetylene composition are very strong at those altitudes. We will concentrate on effects that appear higher in the stratosphere. In the region between approximately 0.1 and 0.01 mbar (300 to 400 km of altitude), the enrichments in composition induce a strong cooling. This effect seems to be present at all latitudes, but with a maximum effect around the winter pole. This may be due to the global differences in the species' distributions between simulations C and R, but also certainly to some thermal horizontal dissipation, with both poles having alternatively lower temperatures. Below this region of cooling, for pressures around 0.5–1 mbar, the thermal effect appears to be reversed, with a region of small heating around the winter pole.

Overall, the changes in temperature due to the composition variations, compared to the reference simulation (or the simulations by Luz et al., 2002), are significant in the mesosphere (above the 0.1 mbar level) and small in the stratosphere. In this region, these changes tend to modify only slightly the fit obtained in Rannou et al. (2002a,b) and Luz et al. (2002) to the temperature latitudinal profiles retrieved from Voyager observations (Fig. 5). In the mesosphere (above 0.1 mbar), our simulations are both significantly warmer than the Lellouch et al. (1990) and Yelle (1991) models. The inclusion of more realistic vertical distributions of ethane and acetylene, and also the inclusion of HCN in the radiative calculations, tend to lower the mesospheric temperatures in the GCM. All the other dynamical fields (e.g., the zonal and meridional winds) are only slightly affected by the variations of composition.

3.2. Cooling rates

The variations of the composition between (and within) the simulations affect the calculation of the cooling rates Q. To compare the cooling rates between the simulations, Q_C and Q_R were computed using a single temperature field (simulation C, northern spring equinox) to focus on effects due to compositions in simulations C and R at the corresponding season. In order to compare the effects of ethane and acetylene variations, we also calculated the cooling rate Q_{C_1}, (respectively Q_{C_2}) using the distribution of ethane (respectively acetylene) from simulation C, and a distribution for the other species uniform in latitude, equal to the equatorial profile from simulation C. As discussed previously in Section 2.1, results above 0.01 mbar should be taken with caution, since the LTE approximation is not justified above this level, in the uppermost layers of the GCM.

The difference $\delta Q_{CR} = Q_C - Q_R$ is shown in Fig. 6a and can be compared to δT_{CR} from Fig. 4a. Vertical profiles of the relative difference with Q_R for Q_{C_1} and Q_{C_2} are plotted for 80°N latitude in Fig. 6b. Ethane has small variations, but has a strong effect on the cooling rate. Acetylene variations are larger, with a weaker effect. Altogether, the variations of the two species' mole fractions induce similar cooling rate variations. The cooling effect above 0.1 mbar and the slight heating below are both visible in these two figures.

For a given pressure, the cooling rate can be separated into three terms: cooling to space, cooling to the surface,

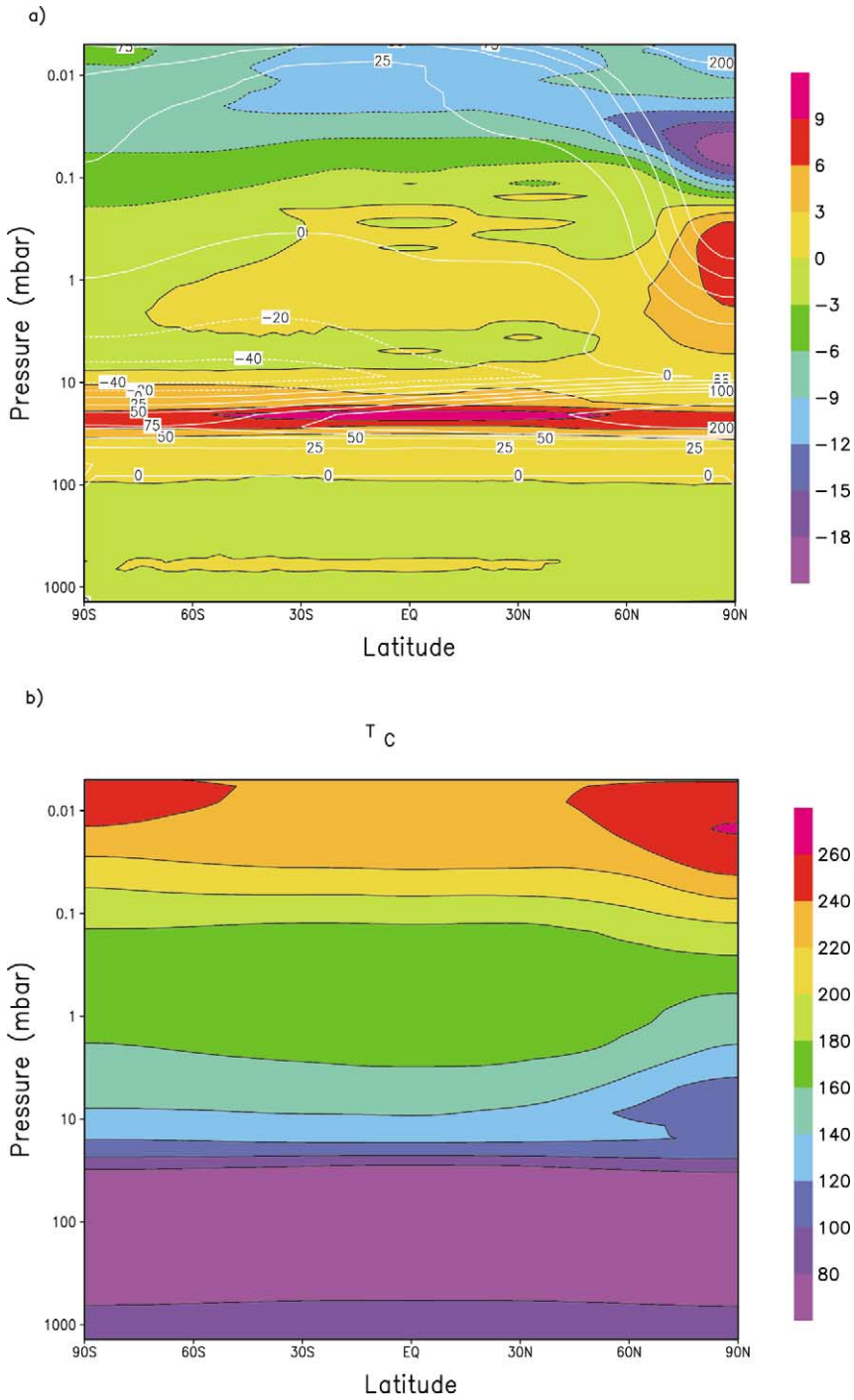

Fig. 4. (a) The difference between the temperature fields of simulations C and R ($\delta T_{CR} = T_C - T_R$) is shown in gray shades for northern spring equinox. The enrichment in ethane between the two simulations ($\delta y_{C_2H_6,CR} = 100 \times (y_{C_2H_6,C} - y_{C_2H_6,R})/y_{C_2H_6,R}$) is plotted using white contours. (b) The temperature field T_C is shown for the same period.

and exchange terms with other levels. Distinguishing these terms inside the GCM is difficult, but a rough estimate indicates that the cooling to space is much larger than the cooling to the surface and that it is the dominant term for the regions we study, above 1 mbar. Increasing the mole fraction of ethane (or acetylene) induces two competing effects on the cooling to space: it increases the energy emitted at this level, but it also increases the total opacity between the level and the top boundary. For deeper stratospheric layers, the energy emitted at the level does not increase as much as for the upper levels, whereas the opacity above continously builds up as altitude decreases. This screen effect becomes

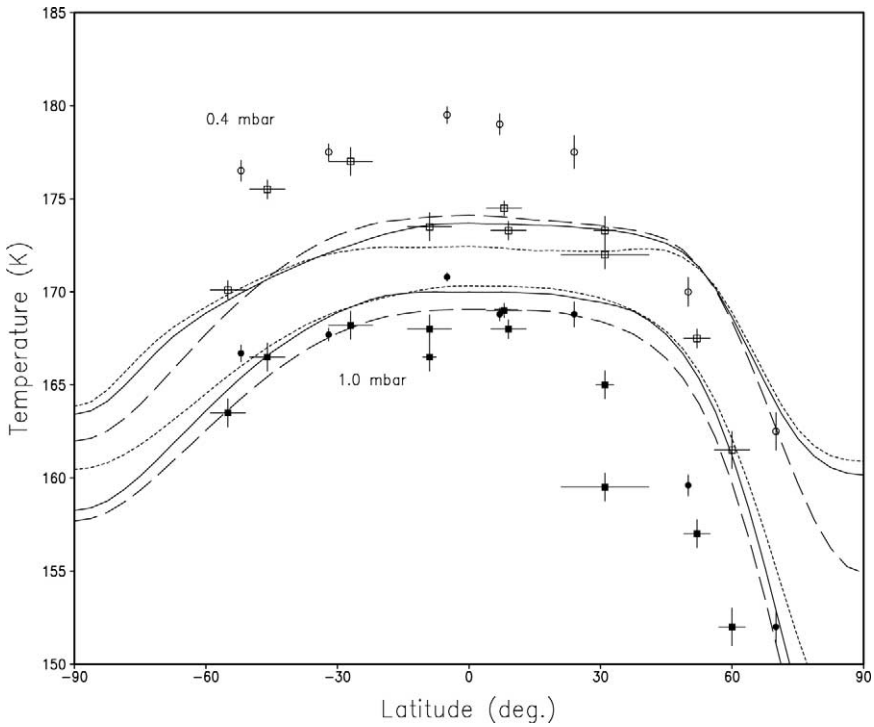

Fig. 5. Latitudinal profiles for the temperature at 0.4 and 1 mbar, plotted for $L_S = 9°$ (season of Voyager 1 fly-by, shortly after northern spring equinox). Comparison between the analysis of IRIS/Voyager 1 data by Flasar and Conrath (1990) (squares, open for 0.4 mbar, black for 1 mbar) and Coustenis and Bézard (1995) (circles), and simulations R (dashed line) and C (solid line) of the GCM. Simulation C′ (dotted line) of the GCM is also shown (see Section 4).

dominant between 0.1 and 1 mbar, which results in the decrease of the cooling to space. The exchange term between the 1 mbar region and the regions above increases (i.e., this region gets heated from above), which may also participate in the resulting heating of this region.

3.3. Comparison with the impact of aerosols

The effect on cooling rates shown in Fig. 6 may also be compared to the impact of aerosol coupling on the global heating rate, as discussed in Rannou et al. (2002b). The aerosols have an effect on both heating and cooling rates. The transport of these aerosols by the circulation induces modification of both, which tend to compensate each other most of the time, except during the winter solstice, at high latitudes. As a mean over the year, the global effect of this coupling is a relative decrease in total heating rates at high latitudes on both poles, compared to a uniform distribution of aerosols. The heating rates decrease by around 35 K/TitanDay (annual mean) from equator to pole in the pressure range 0.3–0.01 mbar. This value is similar to the annual mean increase in cooling rates obtained in this region from the variations of composition (around 40 K/TitanDay). The main difference is that the decrease in heating rates due to aerosol variations affects altitudes down to the 1-mbar level, with a stronger effect than the small cooling rates decrease seen in Fig. 6. This induces that the aerosols have a stronger coupling to the global dynamics than the composition, since dynamics are driven dominantly from low stratospheric levels.

3.4. Seasonal variations

The evolution of this situation during the Titan year is illustrated in Fig. 7, where the temporal evolutions of δT_{CR} and $\delta y_{C_2H_6,CR}$ are plotted as a mean over the pressure range 0.1–0.03 mbar (strongest thermal effect). These differences are correlated to the variations of the ethane (and acetylene) mole fraction, with maximum values correlated to maxima in temperature. The enrichments in the composition are strongest for winter high latitudes, between fall and spring equinoxes, which are closely related to the meridional circulation. The temperature maxima appear seasonally, with the reversal of the circulation. When the ascending region moves from one pole to the other, it induces a variation of the temperature at both poles: first at the spring pole ($L_S \sim 0$–$30°$ and $L_S \sim 180$–$210°$) and shortly after at the fall pole, where the second subsiding region is developing ($L_S \sim 60$–$80°$ and $L_S \sim 240$–$250°$). Adiabatic heating in the subsiding regions together with the variations in insolation around the poles may explain these maxima: at the spring pole, insolation is increasing before the ascending branch reaches the pole, and at the fall pole, increase in temperature may be due to the newly developing subsidence. In both simulations C and R, the ascending region crosses the equator some time after the equinoxes ($L_S \sim 20°$ and $L_S \sim 200°$).

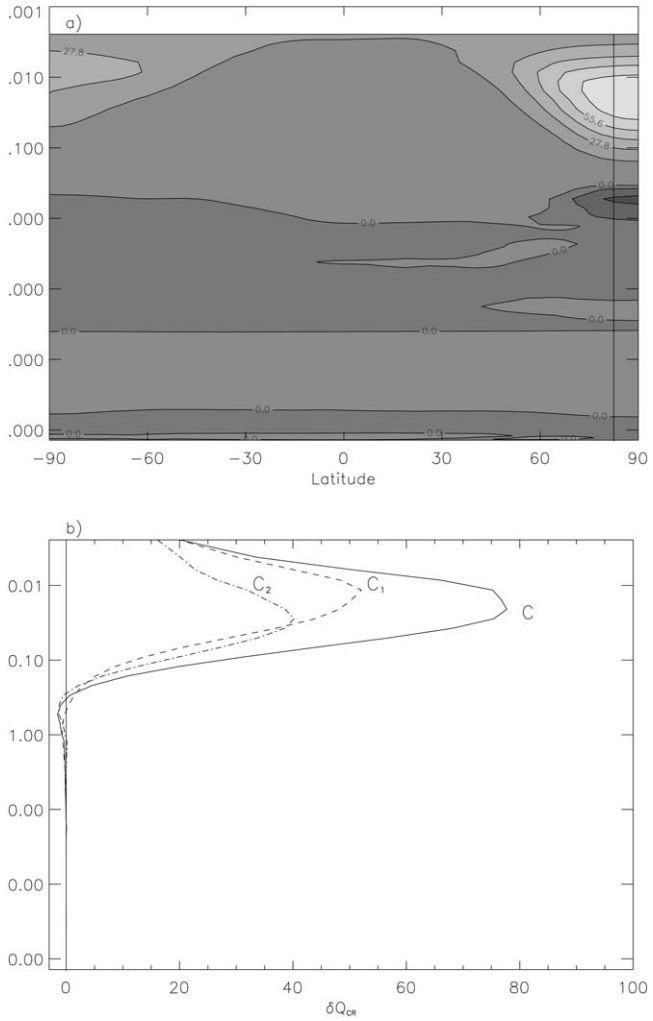

Fig. 6. (a) Variations of the cooling rates $\delta Q_{CR} = Q_C - Q_R$ are plotted for northern spring equinox (in K/TitanDay). The vertical line indicates the latitude 80°N. (b) Vertical profiles of δQ_{CR}, δQ_{C_1R} (only ethane is varying), and δQ_{C_2R} (only acetylene is varying) are plotted for latitude 80°N.

4. Impact of the variations of HCN distribution

As we mentioned earlier, compounds other than ethane and acetylene are suspected to have a seasonal impact on the radiative transfer due to their high enrichment in high-latitude winter conditions, especially HCN and C_4H_2. Including these species in the radiative calculations in the GCM is not straightforward, due to the approach used. The k-distribution exponential-sum band model used (McKay et al., 1989) is mostly valid when only the major absorbing compound is taken into account in each spectral interval. Ethane is used from 740 to 940 cm^{-1} and acetylene from 645 to 740 cm^{-1} (its absorption is neglected in the 740- to 815-cm^{-1} range). A complete modification of the radiative model was beyond the scope of this study. In order to test the possible effects of HCN variations, we used the k-distribution exponential-sum band model for HCN from 645 to 740 cm^{-1} (Table 1) and simply added the absorption to the one calculated for C_2H_2. This rough first approximation has been done to evaluate the possible impact of the strong enhancement observed for some species.

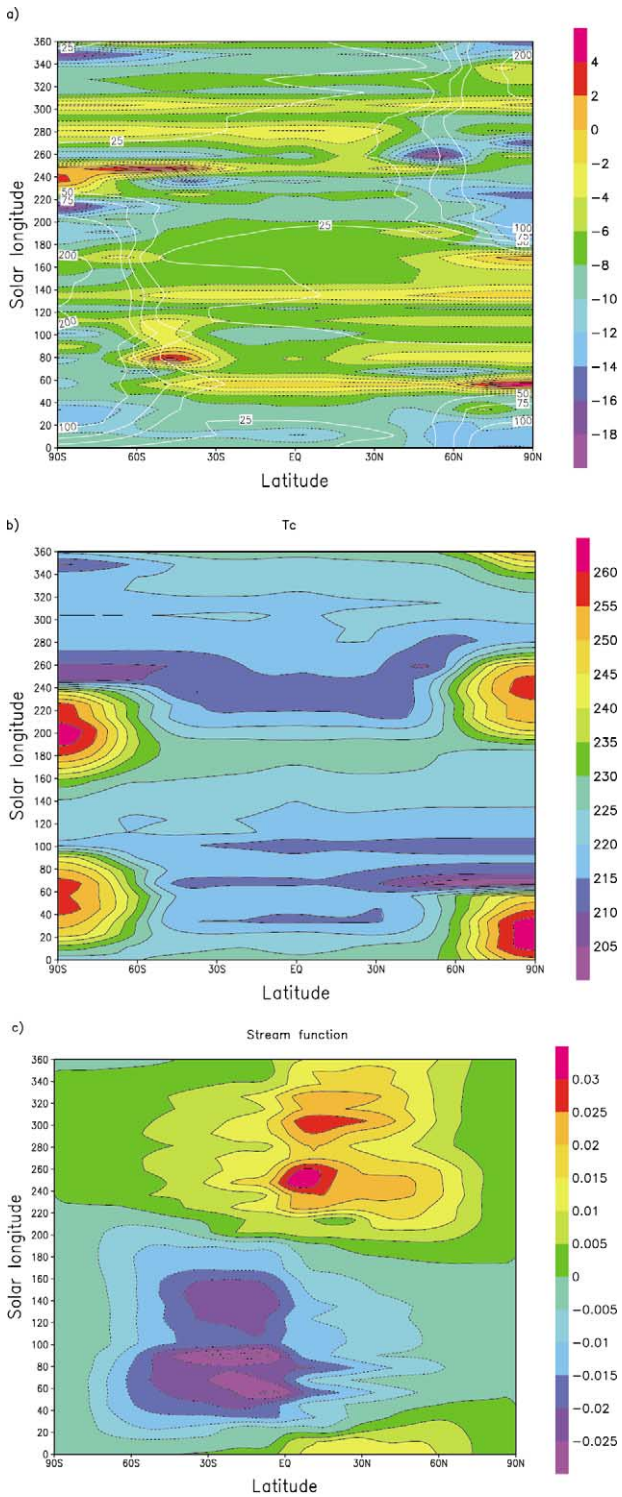

Fig. 7. Mean temporal variations over the pressure range 0.1–0.03 mbar: (a) δT_{CR} and $\delta y_{C_2H_6,CR}$ (same conventions as in Fig. 4a), (b) temperature T_C, and (c) horizontal cut of the meridional stream function for simulation C (unit is 10^9 kg s^{-1}).

Table 1
Spectral intervals and exponential-sum absorption coefficients for hydrogen cyanide

Interval (cm^{-1})	Weight	a_1	a_2	a_3	b_1	b_2	b_3	c_1	c_2	c_3
645–685	0.03334	−33.417	11.425	−2.205	−1.148	2.241	−0.692	−0.415	0.350	−0.087
	0.07473	−35.361	12.367	−2.467	0.907	0.495	−0.239	5.428	−5.785	1.480
	0.10954	−26.098	2.474	−0.050	7.279	−5.124	1.040	−10.563	9.745	−2.251
	0.13463	−39.781	15.474	−3.201	3.607	−1.092	0.007	1.428	−2.336	0.708
685–720	0.03334	−19.761	2.432	−0.665	1.022	−0.802	0.214	1.788	−2.046	0.550
	0.07473	−16.452	−2.787	0.787	−0.336	1.428	−0.452	−0.842	0.789	−0.198
	0.10954	−13.093	−6.367	1.545	−3.111	4.460	−1.197	−3.687	2.985	−0.608
	0.13463	−18.849	−0.492	−0.056	−2.645	4.384	−1.217	4.970	−6.433	1.849
720–740	0.03334	−18.605	1.001	−0.334	−0.667	0.882	−0.206	0.463	−0.695	0.198
	0.07473	−13.479	−4.955	1.081	−5.963	6.788	−1.675	−5.466	5.104	−1.194
	0.10954	−20.717	2.042	−0.731	−1.766	2.827	−0.707	3.148	−4.087	1.177
	0.13463	−17.126	−2.013	0.242	−1.602	2.697	−0.624	−2.218	1.574	−0.309

Though this introduction of HCN in the radiative calculations is only done in an approximate way, we conducted a third simulation in similar conditions to simulation C, but taking HCN into account (simulation C′). This simulation can be compared to the reference simulation and also to simulation C to give a first-order estimation of the role of HCN. In simulation C′, the distributions of ethane and acetylene are almost identical to those in simulation C. The stratospheric distribution of HCN is compared to Voyager observations in Fig. 8.

Fig. 9a shows the difference $T_{C'R}$ and yields very similar conclusions to Fig. 4a. The differences are due to the introduction of HCN in the radiative calculations. The effects of HCN between simulations C and C′ are shown in Fig. 9b, together with the meridional distribution of HCN at northern spring equinox. It mainly induces a global cooling around 0.1 mbar of approximately −5 K. This effect is due to the average level of HCN, and the impact of the seasonal enrichment of HCN is not obvious.

In Fig. 10, we show the relative effect of each constitutent on the cooling rates, calculated for simulation C′ in a similar way as for simulation C (Fig. 6). The effect of HCN ($\delta Q_{C_3'R}$) is comparable here to the effect of C_2H_2.

The radiative role of minor constituents of Titan's stratosphere other than ethane and acetylene has been neglected in the Titan GCM developed since Hourdin et al. (1995).

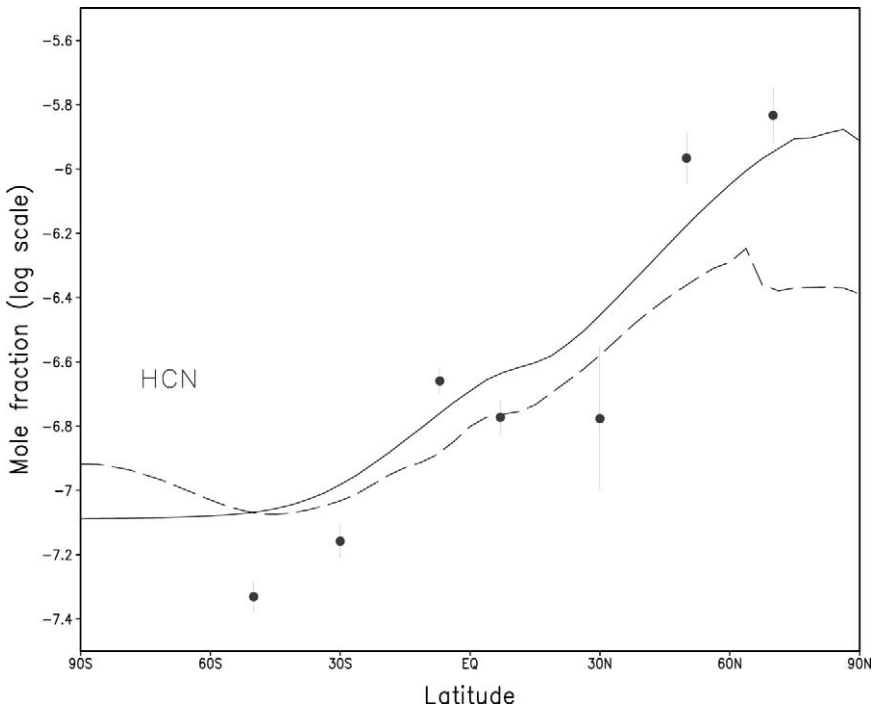

Fig. 8. Same as Fig. 3 for hydrogen cyanide, at a pressure level around 9 mbar.

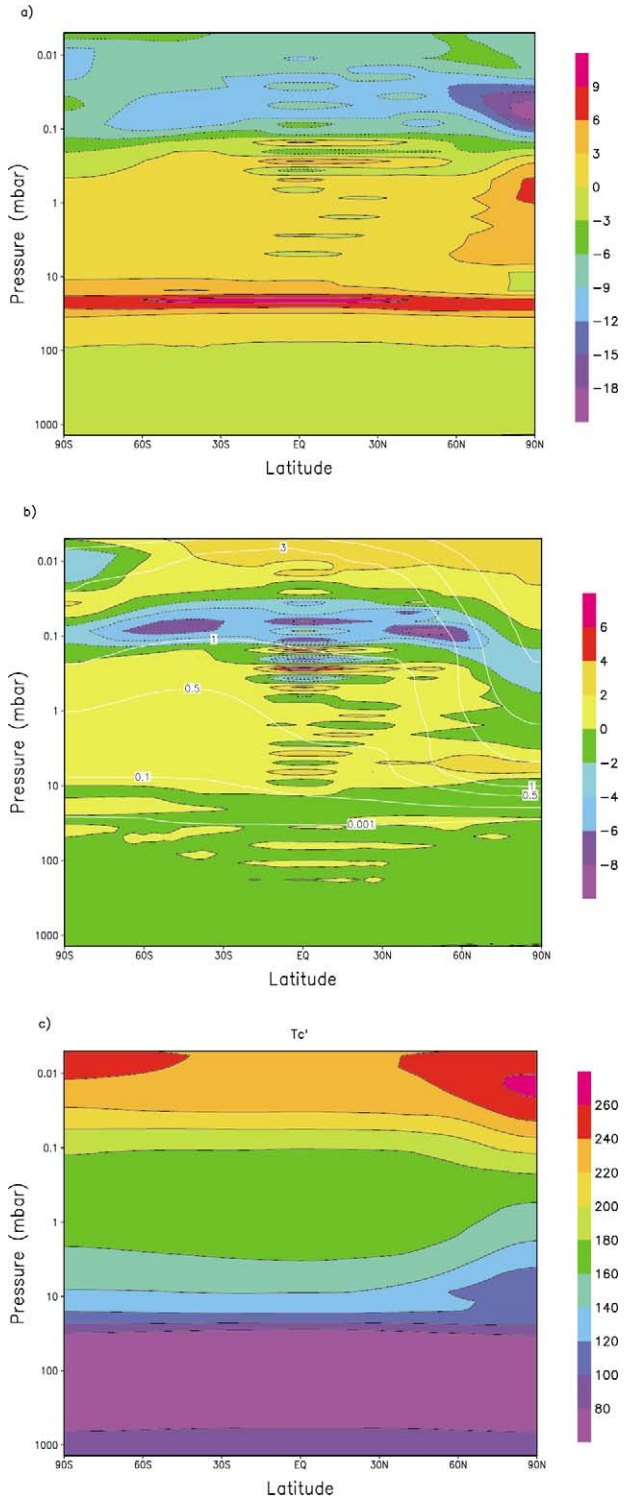

Fig. 9. The differences between the temperature fields of (a) simulations C′ and R ($\delta T_{C'R} = T_{C'} - T_R$), and (b) simulation C′ and C ($\delta T_{C'C} = T_{C'} - T_C$) are shown in gray shades for northern spring equinox, together with the distribution of HCN from simulation C′ (white contours, in ppm). (c) Temperature field C′ is shown for the same period.

This choice was based on the equatorial composition of the stratosphere, as deduced from Voyager observations. Our results discussed here indicate that the introduction of other minor species (e.g., HCN and C_4H_2) may also have a radiative effect. Considering their strong enhancement in high latitudes in winter, the cooling effects induced by HCN and C_4H_2 may become significant in these conditions, as it was also shown in Bézard et al. (1995). We plan to include more components within the radiative calculations of the GCM in the future, for which a revised version of the cooling rates calculations will be necessary.

5. Conclusion

Using our general circulation model that includes chemical tracers, we were able to reproduce the latitudinal variations of ethane, acetylene, and hydrogen cyanide, as observed by IRIS/Voyager 1 in the lower stratosphere. We have studied the effect of the seasonal variations of these compounds' distributions on the temperature field, and the conclusions of this study are the following:

1. At high latitudes between fall and spring, the enhancement of the mole fractions of acetylene and ethane induces a relative decrease in the atmospheric temperature for altitudes above approximately 250 km (pressures lower than ∼0.2 mbar). Lower in the stratosphere, the effect is a small increase. The peak amplitude of the temperature decrease is around −20 K, while the peak amplitude of the increase is around +7 K.
2. These effects are mostly due to the variations of the cooling to space.
3. Including HCN in the radiative calculations induces similar effects. Ethane has a stronger impact than acetylene or HCN on the cooling rate, but its variations are smaller. Therefore, the variations of the three compounds' mole fractions induce similar variations

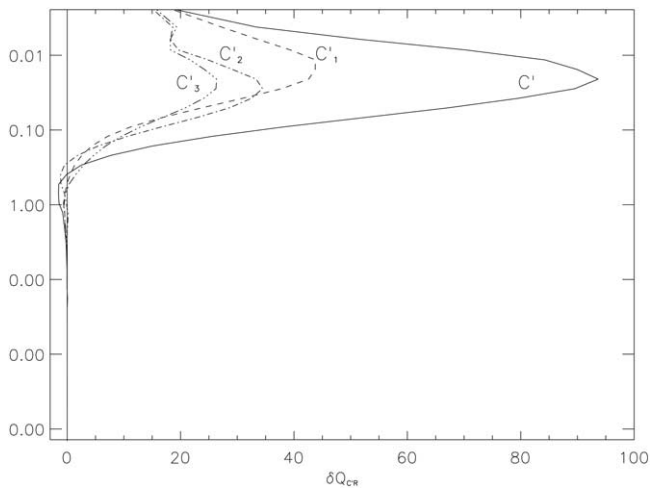

Fig. 10. Vertical profiles of $\delta Q_{C'R}$, $\delta Q_{C'_1R}$ (only ethane is varying), $\delta Q_{C'2R}$ (only acetylene is varying), and $\delta Q_{C'_3R}$ (only HCN is varying) are plotted for latitude 80° N (in K/TitanDay).

in the cooling rate. Although minor compounds other than ethane and acetylene (e.g., HCN and C_4H_2) have been neglected in previous GCM studies, their radiative impact may not be negligible in high-latitude winter conditions, due to their strong observed enhancement.

4. The effect of seasonal variations of the gas composition on the total heating rate is similar to the impact of the coupling between aerosols and the general circulation (Rannou et al., 2002a,b) in the mesosphere (above 0.1 mbar), but is smaller in the stratosphere, around the 1-mbar level. Therefore, it appears that the temperature profiles obtained in the stratosphere from Voyager observations are mainly due to the coupling between aerosols and dynamics, rather than to the seasonal variations of atmospheric composition. The inclusion of ethane, acetylene, and hydrogen cyanide seasonal variations in the radiative calculation of the GCM does not significantly improve the fit to these observed stratospheric temperature profiles that was obtained in previous versions of our GCM (Rannou et al., 2002a,b; Luz et al., 2002). These works support the hypothesis formulated by Bézard et al. (1995) that the characteristics of these observed stratospheric temperature profiles are due to seasonal variations of the opacity sources.

Acknowledgments

This work was performed while S. Lebonnois held a National Research Council Research Associateship Award at NASA Ames Research Center. The authors thank Chris McKay for the HCN data displayed in Table 1.

References

Bézard, B., Coustenis, A., McKay, C.P., 1995. Titan's stratospheric temperature asymmetry: a radiative origin? Icarus 113, 267–276.

Cabane, M., Rannou, P., Chassefière, E., Israel, G., 1993. Fractal aggregates in Titan's atmosphere. Planet. & Space Sci. 41 (4), 257–267.

Coustenis, A., Bézard, B., 1995. Titan's atmosphere from Voyager infrared observations. IV. Latitudinal variations of temperature and composition. Icarus 115, 126–140.

Coustenis, A., Bézard, B., Gautier, D., 1989. Titan's atmosphere from Voyager infrared observations. I. The gas composition of Titan's equatorial region. Icarus 80, 54–76.

Coustenis, A., Bézard, B., Gautier, D., Marten, A., Samuelson, R., 1991. Titan's atmosphere from Voyager infrared observations. III. Vertical distributions of hydrocarbons and nitriles near Titan's north pole. Icarus 89, 152–167.

Flasar, F.M., Conrath, B.J., 1990. Titan's stratospheric temperatures: a case for dynamical inertia? Icarus 85, 346–354.

Hourdin, F., Talagrand, O., Sadourny, R., Courtin, R., Gautier, D., McKay, C.P., 1995. Numerical simulation of the general circulation of the atmosphere of Titan. Icarus 117, 358–374.

Lebonnois, S., Toublanc, D., Hourdin, F., Rannou, P., 2001. Seasonal variations in Titan's atmospheric composition. Icarus 152, 384–406.

Lellouch, E., Hunten, D.M., Kockarts, G., Coustenis, A., 1990. Titan's thermosphere profile. Icarus 83, 308–324.

Luz, D., Hourdin, F., Rannou, P., Lebonnois, S., 2002. Latitudinal transport by barotropic waves in Titan's stratosphere. II. Results from a coupled dynamics-microphysics-photochemistry GCM. Icarus, submitted for publication.

McKay, C.P., Pollack, J.B., Courtin, R., 1989. The thermal structure of Titan's atmosphere. Icarus 80, 23–53.

Rannou, P., McKay ,C.P., 2002. Titan haze vertical structure deduced from the visible geometric albedo. Icarus, submitted for publication.

Rannou, P., Cabane, M., Chassefière, E., Botet, R., McKay, C.P., Courtin, R., 1995. Titan's geometric albedo: role of the fractal structure of the aerosols. Icarus 118, 355–372.

Rannou, P., Hourdin, F., McKay, C.P., 2002. A wind origin for Titan's haze structure. Nature 418, 853–856.

Yelle, R.V., 1991. Non-LTE models of Titan's upper atmosphere. Astrophys. J. 383, 380–400.